Intercomparison of methods of coupling between convection and large-scale circulation. 2: Comparison over non-uniform surface conditions

C. L. Daleu[1], R. S. Plant[1], S. J. Woolnough[2], S. Sessions[3], M. J. Herman[3],

A. Sobel[4], S. Wang[5], D. Kim[6], A. Cheng[7], G. Bellon[8],P. Peyrille[9], F. Ferry[9],

P. Siebesma[10,11], and L. van Ulft[10]

Correspondence to: C. L. Daleu, c.daleu@reading.ac.uk

[1]Department of Meteorology, University

Abstract. As part of an international intercomparison project, the two-way interaction between convection and large-scale dynamics is studied in a set of single column models (SCMs) and cloud-resolving models (CRMs) using two large-scale parameterization methods: the weak temperature gradient (WTG) method and the damped gravity wave (DGW) method. For each model, the implementation of the WTG or DGW method involves a simulated column which is coupled to a reference state defined with profiles obtained from the same model in radiative-convective equilibrium. In Part 1 of this study, the simulated column has the same sea surface temperature (SST) as the reference state. In this paper, the reference state is held fixed while the SST in the simulated column is varied. For each value of SST, we performed two sets of systematic comparisons: a comparison of the WTG and DGW methods with a consistent implementation in models with different physics and numerics, and a comparison of the behavior of those models using the same large-scale parameterization method.

The sensitivity of precipitation rate to the SST differs from model to model and also depends on whether the WTG or DGW method is used to parameterize the large scale circulation. In general, SCMs display a wider range of behaviors than CRMs. CRMs show a fairly linear relationship between precipitation and circulation strength, but a few SCMs deviate from this linear relationship. All CRMs using either the WTG or DGW method show a nonlinear increase of mean precipitation rate with SST. In contrast, SCMs

of Reading, Reading, UK,

show sensitivities of the mean precipitation rate to the SST which are not always monotonic. Within an individual SCM, a WTG simulation and a corresponding DGW simulation can produce different signs of the circulation. In general, DGW simulations produce large-scale pressure velocity profiles which are smoother and less top-heavy compared to those produced by the WTG simulations.

Consistent with observations and other numerical model studies, precipitation rate increases with column-relative humidity. A large proportion of the models show a rapid increase of mean precipitation rate when column-relative humidity increases pass a threshold value. CRMs using either the WTG or DGW method show very similar relationships between mean precipitation rate and column-relative humidity, while SCMs exhibit a much wider range of behaviors.

---

[2]National Centre for Atmospheric Science,

1. Introduction

A key issue in understanding the tropical climate and its variability is the understanding of the two-way interaction between tropical deep convection and large-scale tropical circulations. Numerical models which simultaneously simulate convection and large-scale circulations are computationally expensive due to the large range of spatial scales between individual convective cells and large-scale tropical circulations. Some examples include large-domain, high-resolution simulations as those conducted in projects such as Cascade [e.g. *Holloway et al.*, 2012].

In the past decade, various forms of parameterized large-scale dynamics have been developed to study the two-way interaction between deep convection and large-scale dynamics at a reasonable computational cost in both single column models (SCMs) and cloud-resolving models (CRMs). Parameterized large-scale dynamics is a set of methods developed to capture the feedbacks of large-scale dynamics on convection and vice versa, in a way broadly consistent with our physical understanding of the large-scale tropical atmosphere. This study compares two methods of parameterized the large-scale dynamics–the weak-temperature gradient (WTG) method and the damped gravity wave (DGW) method–in a set of CRMs and SCMs.

The WTG method relies on the physical principle that gravity waves act to redistribute local buoyancy anomalies in the free troposphere [*Bretherton and Smolarkiewcz*, 1989; *Mapes and Houze*, 1995; *Yano and Bonazzola*, 2009] and thus, maintain nearly uniform horizontal temperature gradients near the equator where the action of the Coriolis force

Department of Meteorology, University of

is small. The WTG method has been applied to parameterize large-scale tropical circulations that either consume the simulated heating and accordingly maintain zero horizontal temperature gradient [*Sobel and Bretherton*, 2000] or remove the horizontal temperature gradient over a short but nonzero time-scale [e.g., *Raymond and Zeng*, 2005; *Sessions et al.*, 2010; *Daleu et al.*, 2012; *Sessions et al.*, 2015]. A recent innovation of the WTG method involves spectral decomposition of heating in the vertical dimension [*Herman and Raymond*, 2014].

The DGW method derives the large-scale vertical velocity directly from the approximated momentum equations. This large-scale parameterization method has been applied in several studies that simulate the two-way coupling between convection and large-scale dynamics, with the latter being simplified to a linear gravity wave of a single horizontal wavenumber [*Kuang*, 2008, 2011; *Wang et al.*, 2013; *Romps*, 2012a, b; *Edman and Romps*, 2015].

The implementation of the WTG and DGW methods has always required a reference state that is coupled to the simulated column [e.g., *Raymond and Zeng*, 2005; *Sobel et al.*, 2007; *Sessions et al.*, 2010; *Wang and Sobel*, 2011; *Kuang*, 2008, 2011; *Wang and Sobel*, 2012; *Wang et al.*, 2013; *Romps*, 2012a, b]. Recently, however, *Daleu et al.* [2012] developed a new configuration that couples two simulated columns via a WTG-derived large-scale circulation to study the influence on local convection due to changes in remote convection [*Daleu et al.*, 2014]. Much insight has been learned from these efforts. Unfortunately, many aspects of the large-scale parameterization methods remain uncertain since results using these two large-scale parameterization methods show both sim-

Reading, Reading, UK,

ilarities and discrepancies in model behavior. In order to understand the different behaviors of these large-scale parameterization methods, this international intercomparison project–the GASS-WTG project–was developed by the Global Energy and Water Exchanges (GEWEX) Global Atmospheric Systems Modelling Panel (GASS). The goals of this project are to develop community understanding of the WTG and DGW methods, to identify differences in behavior of SCMs compared to CRMs to inform parameterization development, and to assess the usefulness of these approaches as tools for parameterization development.

In Part 1 of this study [*Daleu et al.*, 2015], the aim was to understand what causes discrepancies in model behavior when surface conditions in the simulated column are identical to those of the reference state. We implemented the WTG and DGW methods in a set of CRMs and SCMs. For each model, the reference state was defined from profiles obtained in the radiative-convective equilibrium (RCE) simulation of that model. WTG and DGW simulations were performed with the same SST as in the reference state and were initialized with profiles from the reference state. Some models produced an equilibrium state which was almost identical to the corresponding RCE reference state. In contrast, other models developed a large-scale circulation which resulted in either substantially higher or lower precipitation rates in the simulated column compared to the implied value for the RCE reference column. We also explored the sensitivity of the final equilibrium state to the initial moisture conditions. We found that while some models are not sensitive to the initial moisture conditions (independent of the method

[3]Department of Physics, New Mexico

used to parameterize the large-scale circulation), other models may support two distinct precipitating equilibrium states using either the DGW or WTG method. We also found

Tech, Socorro, New Mexico, USA,

[4]Department of Environmental Sciences, Columbia University, New York, New York, USA,

[5]Department of Applied Physics and Applied Mathematics, Columbia University, New York, New York, USA,

[6]Department of Atmospheric Sciences, University of Washington, Seattle, Washington, USA,

[7]Climate Science Branch, NASA Langley Research Centre, Hampton, Virginia, USA,

[8]The Department of Physics, University of Auckland, Auckland, New Zealand,

[9]Meteo France, Toulouse, France,

[10]Royal Netherlands Meteorological Institute, De Bilt, Netherlands.

[11]Delft University of Technology, Delft, Netherlands

that some models using the WTG method (but not using the DGW method) can support either an equilibrium state with persistent, precipitating convection or an equilibrium state with zero precipitation.

Daleu et al. [2015] revealed some weaknesses of the WTG method. For instance, over uniform SST, the existence of the nonprecipitating equilibrium state in some models was sensitive to the choice of the parameters used in the WTG calculations (e.g., the nominal boundary layer depth). In addition, DGW simulations over uniform SST and with uniform radiative forcing were more likely to reproduce the RCE reference conditions and produced large-scale pressure velocities which were smoother compared to those produced by the WTG simulations. Aside from the choice of the large-scale parameterization method and the details of its implementation, various other factors in the convective models were important for the evolution of convection and its interactions with parameterized large-scale dynamics. For instance, we found that CRMs using either the WTG or DGW method produced broadly similar results, while SCMs produced a much wider range of behaviors.

Whilst *Daleu et al.* [2015] considered the case where the simulated column had the same SST as the RCE reference state, this paper focuses on the sensitivity to the SST in the simulated column, which has been a major focus of previous studies using these approaches [e.g., *Raymond and Zeng*, 2005; *Sobel et al.*, 2007; *Wang and Sobel*, 2011]. In the present study, we use the same set of CRMs and SCMs presented in *Daleu et al.* [2015]. For each model, we fix the reference state and perform a series of WTG and DGW simulations with a range of SSTs in the simulated column. We perform systematic comparisons of the WTG and DGW methods with a consistent implementation in the

models, and also systematic comparisons of the behavior of the models given the same large-scale parameterization method.

This paper is organized as follows. Section 2 briefly describes the models that have contributed to this study. Section 3.1 outlines our implementation of the WTG and DGW methods (full details are available in *Daleu et al.* [2015]), while Section 3.2 describes the configurations of our numerical simulations. Section 4 compares the results of the WTG and DGW simulations over non-uniform SSTs. Finally, the conclusions and implications of our study are discussed in section 5.

2. Models description

Six groups participating in this intercomparison study performed simulations with the same set of models presented in *Daleu et al.* [2015]. There are 12 models, including five CRMs (two in three-dimensions [3-D] and three in two-dimensions [2-D]) and seven SCMs. The models are listed in Tables 1 and 2 for CRMs and SCMs, respectively.

2.1. Cloud Resolving Models

WRF is the Weather Research and Forecast model version 3.3 [*Skamarock et al.*, 2008], MesoNH is the mesoscale, nonhydrostatic atmospheric model [*Lafore et al.*, 1997], LaRC-CRM is the Langley Research Center Cloud-Resolving Model (LaRC-CRM) [*Cheng and Xu*, 2006], NMTCMv3 is the New Mexico Tech cloud model introduced in *Raymond and Zeng* [2005], with modifications and enhancements described in *Herman and Raymond* [2014], and LEMv2.4 is the Met Office Large Eddy Model at version 2.4 [*Shutts and Gray*, 1994; *Petch and Gray*, 2001]. The reader is referred to *Daleu et al.* [2015] for a more complete description of these CRMs.

2.2. Single-Column Models

Two pairs of these SCMs are different versions of the same atmospheric model. One of the pairs, LMDzA and LMDzB, are the SCM versions of the atmospheric components of IPSL-CM5A and IPSL-CM5B [*Dufresne et al.*, 2013]. The other pair, EC-Earthv1 and EC-Earthv3, are SCMs based on the atmospheric general circulation model IFS, cycles 31r1 and 36r4 respectively of the European Centre for Medium-Range Weather Forecasts (ECMWF) [*Hazeleger et al.*, 2010]. ARPv6 is the SCM version of the atmospheric component of the CNRM-CM, an updated version from that used in CMIP5 [*Voldoire et al.*, 2013], GISS-SCM is the SCM version of the National Aeronautics and Space Administration Goddard Institute for Space Studies, an updated version from that used in CMIP5 [*Schmidt et al.*, 2014], and UMv7.8 is the SCM version of the UK Met Office Unified Model [*Davies et al.*, 2005]. The reader is referred to *Daleu et al.* [2015] for a more complete description of these SCMs.

2.3. Overall approach

The CRMs have horizontal domain sizes ranging between 128 and 256 km and horizontal resolution ranging between 0.5 and 4 km. For each CRM, the domain is not so large as to allow spontaneous mesoscale organization of convection [*Tompkins*, 2000; *Bretherton et al.*, 2005]. The lateral boundary conditions are periodic for all prognostic variables in all CRMs. For CRMs in 2-D, the domain-mean wind speeds in the along-domain direction and in the across-domain direction are relaxed toward vertically uniform values of 0 and 5 m s^{-1}, respectively, both with a relaxation time-scale of 6 h. The along-domain wind is suppressed to avoid the development of along-domain wind shear that may otherwise occur [*Tompkins*, 2000; *Mapes and Wu*, 2001] and encourage the formation of squall lines

[*Robe and Emanuel*, 2001; *Tao et al.*, 1999]. For fair comparison of 2-D CRM simulations with 3-D CRM simulations and with SCM simulations, the horizontal domain-mean wind speed components in the 3-D CRMs and SCMs are also relaxed toward vertically uniform values of 0 and 5 m s^{-1}. Applying a vertically uniform wind speed of 5 m s^{-1} simply increases the value of surface evaporation compared to the no wind case without affecting the dynamics of convection.

For all of these models, the lower boundary condition is a spatially uniform and time-independent SST, and the Coriolis force is zero. We force each model with the idealized cooling profile defined in *Daleu et al.* [2015], so that the tendency of temperature due to radiative cooling $(\partial T/\partial t)_{RC}$ is defined as

$$\left(\frac{\partial T}{\partial t}\right)_{RC} = \begin{cases} -1.5 & \text{if} \quad \overline{p} \geqslant 200 \\ -1.5\left(\frac{\overline{p}-100}{100}\right) - \alpha_T\left(\frac{200-\overline{p}}{100}\right)(\overline{T}-200) & \text{if} \quad 100 < \overline{p} < 200, \\ -\alpha_T(\overline{T}-200) & \text{if} \quad \overline{p} \leqslant 100 \end{cases} \tag{1}$$

where the overbar denotes a horizontal domain-average, p is the pressure in hPa and $\alpha_T^{-1} = 1$ day is the relaxation time-scale of the temperature T toward a fixed value of 200 K at levels with $\overline{p} < 100$ hPa. Equations similar to equation 1 have been used in previous studies [*Pauluis and Garner*, 2006; *Wang and Sobel*, 2011]. It produces radiative cooling which is homogeneous and non-interactive throughout most of the troposphere and depends on temperature above 200 hPa.

3. Parameterization of the large-scale dynamics and experiment setup

3.1. Parameterization of the large-scale dynamics

In the present study, the large-scale circulation is parameterized using two methods: the WTG and DGW methods. As in *Daleu et al.* [2015], the implementation of the WTG or DGW method involves a reference state that is coupled to an interactive column.

To implement the WTG method we generally followed the procedures used in *Raymond and Zeng* [2005], *Sobel et al.* [2007], and *Daleu et al.* [2012]. We diagnose the large-scale pressure velocity, $\overline{\omega}$ in the free troposphere that acts to reduce the difference in the domain-mean virtual potential temperature between the simulated column and the reference state, $\overline{\theta}_v - \overline{\theta}_v^{Ref}$, over a specified time-scale, τ. Thus,

$$\overline{\omega}\frac{\partial\overline{\theta}_v^{Ref}}{\partial p} = \frac{\overline{\theta}_v - \overline{\theta}_v^{Ref}}{\tau}. \tag{2}$$

In the boundary layer, the WTG approximation is not valid because strong surface fluxes create temperature gradients more efficiently than gravity waves damp them [*Sobel and Bretherton*, 2000]. As in *Daleu et al.* [2015], we choose a nominal boundary layer top, p_b, arbitrarily at 850 hPa. We apply equation 2 from the first model level above p_b to 100 hPa, and below p_b we calculate the values of $\overline{\omega}$ by linear interpolation in pressure from the value diagnosed at the first model level above p_b to zero at the surface. Experiments to assess sensitivities of the final equilibrium state to the depth of the boundary layer are presented in *Daleu et al.* [2015]. A full description of the implementation of the WTG method used in this study is given in *Daleu et al.* [2015].

The DGW method is applied to couple convection and large-scale dynamics with the latter being simplified to a linear gravity wave of a single horizontal wavenumber. To implement the DGW we generally followed the procedures of *Kuang* [2008], and *Kuang* [2011]. We derive $\overline{\omega}$ from a wave equation that is obtained by combining the momentum and thermodynamics equations. The second-order derivative of $\overline{\omega}$ is related to the difference in the domain-mean virtual temperature between the simulated column and the

reference state, $\overline{T_v} - \overline{T}_v^{Ref}$, as

$$\frac{\partial}{\partial p}\left(\epsilon\frac{\partial\overline{\omega}}{\partial p}\right) = \frac{k^2 R_d}{\overline{p}^{Ref}}(\overline{T}_v - \overline{T}_v^{Ref}), \tag{3}$$

where R_d is the gas constant of dry air. ϵ and k are the mechanical damping coefficient and the horizontal wavenumber, respectively, and $\overline{p}^{Ref}$ is the domain-mean pressure of the reference state.

The large-scale circulation parameterized using either equation 2 or 3 introduces additional source and sink terms to the heat and moisture budgets. As in *Daleu et al.* [2015], the effect of the diagnosed large-scale pressure velocity is considered on potential temperature and water vapor only. The prognostic equation for potential temperature includes the tendency due to vertical advection by the parameterized large-scale circulation. That is,

$$\left(\frac{\partial\theta}{\partial t}\right)_{LS} = -\overline{\omega}\frac{\partial\overline{\theta}}{\partial p}. \tag{4}$$

The prognostic equation for specific humidity of water vapor (q_v) also includes the large-scale tendency due to vertical advection, as well as an additional contribution representing the horizontal advection of the reference state air into the simulated domain by the parameterized large-scale circulation. That is,

$$\left(\frac{\partial q_v}{\partial t}\right)_{LS} = -\overline{\omega}\frac{\partial\overline{q}_v}{\partial p} + max\left(\frac{\partial\overline{\omega}}{\partial p}, 0\right)(\overline{q}_v^{Ref} - \overline{q}_v), \tag{5}$$

where $\overline{q}_v^{Ref}$ is the specific humidity of the reference state. The second term on the right hand side of equation 5 is described as "lateral entrainment" by *Raymond and Zeng* [2005].

3.2. Experiment Setup

For each model, a radiative-convective equilibrium (RCE) simulation (no large-scale parameterized dynamics) is first performed over an SST of 300 K. The mean thermody-

namic profiles at equilibrium in that simulation are used to define the reference state of that model. We keep the reference state fixed and investigate the sensitivity of the final equilibrium state to the SST in the simulated column as in *Wang and Sobel* [2011].

For each of the models listed in Tables 1 and 2, we performed the WTG and DGW simulations of a colder column (using SSTs of 298 and 299.5 K), a warmer column (using SSTs of 300.5, 301, 301.5 and 302 K), and over a uniform SST (using an SST of 300 K; results presented in *Daleu et al.* [2015]).

The adjustment time-scale used in the WTG calculations is $\tau = 3$ h. In the DGW calculations, we fix the value of ϵ to 1 day^{-1} and solve equation 3 with a single horizontal wavenumber $k = 10^{-6}$ m^{-1}. These are typical values used in previous WTG and DGW studies [e.g., *Herman and Raymond*, 2014; *Daleu et al.*, 2012; *Wang and Sobel*, 2011; *Wang et al.*, 2013], including *Daleu et al.* [2015]. They have been chosen such that the WTG simulation and the corresponding DGW simulation produce large-scale circulations that are comparable in strength for similar temperature anomalies. The calculations of $\overline{\omega}$ given by equations 2 and 3 are performed either every 10 min (for models with integration time steps smaller or equal to 10 min) or at every model time step (for models with integration time steps greater than 10 min).

The results presented in *Daleu et al.* [2015], and in other previous studies [e.g., *Sobel et al.*, 2007; *Sessions et al.*, 2010] show that some SCMs and CRMs using the WTG method can sustain either a dry equilibrium state or a precipitating equilibrium state, given sufficiently different initial moisture conditions (known as multiple equilibria). Therefore, it is possible that some of our WTG simulations that exhibit precipitating equilibrium states would instead result in dry equilibrium states if initialized with very dry moisture condi-

tions. Multiple equilibria and their dependence on parameters in the WTG calculations have already been investigated in *Daleu et al.* [2015], and they are outside the scope of the present paper.

The WTG and DGW calculations are initialized with profiles from the models RCE reference state at 300 K and are allowed to evolve until a new quasi-equilibrium state with parameterized large-scale circulation is reached. The RCE reference profiles differ from model to model, with large differences obtained among SCMs (see Figure 3 in *Daleu et al.* [2015]). The value of surface sensible heat flux also differs between models (not shown) but is much smaller than surface latent heat flux, such that the main balance in the RCE state is between the precipitation rate and the column-integrated radiative cooling rate. Due to the dependence of radiative cooling profile on temperature above 200 hPa (see equation 1), the value of column-integrated radiative cooling rate differs from model to model. For example, in *Daleu et al.* [2015] we found that ARPv6 produces the smallest column-integrated radiative cooling rate and has a significant lower mean precipitation rate compared to all other models. The values of mean precipitation rate obtained in the RCE simulations with an SST of 300 K are summarized in the last rows of Tables 1 and 2 for CRMs and SCMs, respectively.

We conducted a set of WTG and DGW simulations over non-uniform SSTs using each of the models listed in Tables 1 and 2. The simulations are integrated over different periods of time ranging between 50 and 250 days, as the time-scale of adjustment to a quasi-equilibrium state with the parameterized large-scale circulation differs from model to model and also depends on which large-scale parameterization method is used (not shown). The mean states and statistics at equilibrium of the simulations to be discussed

have been obtained by averaging over a period of time such that a statistically steady state can be defined. The averaging periods were the last 20 days in 50-day simulations, 30 days in 100-day simulations, and 100 days in 250-day simulations.

4. Results

In this section, we present the profiles of large-scale pressure velocity and the values of precipitation at equilibrium for different values of SST in the simulated column. We also present the mean values of precipitation, circulation strength, and column-relative humidity in a set of scatter plots to characterize the response of convection to changes in surface conditions.

4.1. Precipitation and parameterized large-scale circulation

Figures 1 and 2 show the profiles of $\overline{\omega}$ obtained at equilibrium in the WTG and DGW simulations, respectively. Results are shown for all models listed in Tables 1 and 2 and for SSTs of 298, 299.5, 300 K (uniform SST; results presented in *Daleu et al.* [2015]), 300.5, 301, 301.5 and 302 K. For models in height coordinates, we expressed the large-scale vertical velocities in Pa s^{-1} by applying the factor "$-\rho g$," where ρ is density and g is the gravitational acceleration.

To provide a more quantitative evaluation of the WTG and DGW simulations, we calculated the ratio of mean precipitation rate in the simulated column, P, to the value of the corresponding RCE reference state, P_{Ref}. We also calculated the mass-weighted vertical integral of the large-scale pressure velocities presented in Figures 1 and 2; $\Omega = \int \overline{\omega} dp/\Delta p$, where Δp is the depth of the troposphere. The numerical values of Ω and P/P_{Ref} are listed in Tables 3 and 4 for CRMs and SCMs, respectively. Figure 3 shows

P/P_{Ref} as a function of the SST in the simulated column, and Figure 4 shows scatter plots of Ω versus P/P_{Ref} for all SSTs.

4.1.1. Variations between models

For a given SST in the simulated column, the characteristic vertical structure of the large-scale circulation at equilibrium differs from model to model, and it also depends on the large-scale parameterization method used. Over an SST of 302 K (red curves in Figures 1 and 2), for example, models using the WTG method exhibit a range of large-scale pressure velocity profiles which vary from unimodal ascent through the column with very top-heavy profiles (e.g., WRF; Figure 1a), to more uniform unimodal profiles (e.g., LaRC-CRM; Figure 1c), to bi-modal profiles (e.g., EC-Earthv1; Figure 1k), to profiles with distinct minima near the freezing level (e.g., UMv7.8; Figure 1j), including some with weak descent near the freezing level (e.g., GISS-SCM; Figure 1h). As seen in *Daleu et al.* [2015], the DGW method produces large-scale pressure velocity profiles which are smoother than those produced using the WTG method (compare Figures 1 and 2).

Over cold SSTs (298 and 299.5 K), some models produce large-scale pressure velocity profiles which are insensitive to the SST. In such simulations, convection is inhibited completely and the heating due to the diagnosed large-scale circulation balances the prescribed radiative cooling. Some examples are the WTG simulations of LEMv2.4 with SSTs of 298 and 299.5 K which produce zero precipitation rates (see Table 3) and indistinguishable large-scale pressure velocity profiles (see dark blue and light blue curves in Figure 1e).

Over warm SSTs, the large-scale pressure velocity profiles are sensitive to the SST in all the models using either the WTG or DGW method. All CRMs with an SST$\geqslant$ 301 K have large-scale pressure velocities increasing upward to around 400 hPa using the

DGW method and to around 250 hPa using the WTG method. The large-scale pressure velocity profiles produced in most SCM simulations vary considerably from the very top-heavy profiles (e.g. GISS-SCM using the DGW method, see Figure 2h) through weakly top-heavy profiles (e.g. LMDzB using the WTG method, see Figure 1g) to the bottom-heavy profiles (e.g., EC-Earthv1 using the WTG method; see Figure 1k), and some of the pressure velocity profiles show very detailed structures in the vertical (e.g., UMv7.8 using the WTG method; see Figure 1j). Similar to the results of *Wang et al.* [2013], the pressure velocity profiles produced using the DGW method are much smoother and tend to be slightly less top-heavy compared to those produced using the WTG method (compare Figures 1 and 2).

4.1.2. Variations with SST

The impact of the SST is readily seen. At SST= 298 K, all the models using either the WTG or DGW method produce uniform large-scale descent (see the dark blue curves in Figures 1 and 2). In some of these simulations, the large-scale circulation inhibits precipitating convection completely (e.g., NMTCMv3 using the DGW method; see Table 3), while in others an equilibrium state with light precipitation can be achieved (e.g., LMDzB using the WTG method; see Table 4).

At SST= 299.5 K, all CRMs using either the WTG or DGW method produced uniform large-scale descent. With the exception of GISS-SCM using the WTG method, which produces large-scale ascent in the upper troposphere (light blue curve in Figure 1h), the other SCMs produce either a uniform large-scale descent throughout the column (e.g., ARPv6 using the WTG method; light blue curve in Figure 1i) or large-scale descent in the upper troposphere and a very weak circulation in the lower troposphere (e.g., EC-Earthv3

using the WTG method; light blue curve in Figure 1l). The WTG and DGW simulations which produce uniform large-scale descent result in very low precipitation compared to the value of the RCE reference state, consistent with the diminished moisture transport implied by the resulting large-scale circulation (e.g., MesoNH using the WTG method; see Table 3), with some simulations producing zero precipitation at equilibrium (e.g., WRF using the WTG method; see Table 3). The WTG and DGW simulations which produce large-scale descent in the upper troposphere and a very weak circulation in the lower troposphere are dominated by shallow convection and thus, result in smaller reduction in precipitation compared to the value of the RCE reference state (e.g., EC-Earthv3 using the WTG method; see Table 4). However, in the WTG simulation of GISS-SCM with an SST of 299.5 K the mean precipitation rate at equilibrium is slightly increased (with respect to the value of the RCE reference state) to balance the net small cooling produced by the large-scale ascent in the upper troposphere. In contrast, the DGW simulation of GISS-SCM with an SST of 299.5 K produce a different sign of the circulation with a reduction of precipitation (see Table 4).

The results of the WTG and DGW simulations over uniform SST are presented in *Daleu et al.* [2015]. There, we considered that a WTG or DGW simulation over a uniform SST replicated the corresponding RCE reference state to a good approximation if $0.9 < P/P_{Ref} < 1.1$ and $-0.4 \times 10^{-2} < \Omega < 0.4 \times 10^{-2}$ Pa s^{-1}. The values of Ω and P/P_{Ref} for such simulations are both bold-faced in Tables 3 and 4. Some models do replicate the RCE reference state to a good approximation but others sustain a large-scale ascent which results in substantially higher precipitation rate in the simulated column compared

to the value of the corresponding RCE reference state, while others sustain a large-scale descent which results in substantially lower precipitation rate.

Over a uniform SST of 300 K, models which produce a lower precipitation rate will not produce a mean precipitation rate which is equivalent to the value of the RCE reference state unless the SST in the simulated column is increased, consistent with the results of *Raymond and Zeng* [2005]. An example is UMv7.8 using the WTG method (see P/P_{Ref} as a function of the SST; green curve in Figure 3b). Similarly, models which produce a higher precipitation rate will not produce a mean precipitation rate which is equivalent to the value of the RCE reference state unless the SST in the simulated column is decreased (e.g., ARPv6 using the WTG method; solid black curve in Figure 3b).

An SST of 300.5 K results in substantially higher precipitation rate ($P/P_{Ref} > 1.1$) in all the WTG and DGW simulations, except EC-Earthv1. A large proportion of these simulations produce uniform large-scale ascent (e.g., GISS-SCM using the DGW method, dark green curve in Figure 2h). However, other simulations produce large-scale circulations with a layer of descent near the freezing layer, but which result in net cooling and moistening of the simulated column (e.g., ARPv6 using the WTG method, dark green curve in Figure 1i and $P/P_{Ref} > 1.1$ in Table 4). In contrast, the WTG and DGW simulations of EC-Earthv1 with an SST of 300.5 K produce large-scale circulations with ascent in the upper troposphere and descent in the lower troposphere (dark green curves in Figures 1k and 2k), despite producing ascent in the lower troposphere over a uniform SST of 300 K (black curves in Figures 1k and 2k). Using the DGW method, the upper tropospheric cooling and moistening offset the lower tropospheric warming and drying and the mean precipitation rate in the simulated column is maintained close to the value

of the RCE reference state (see Table 4). In contrast, using the WTG method the upper tropospheric cooling and moistening do not prevent a reduction in precipitation rate due to the lower tropospheric warming and drying (see Table 4). A similar result is obtained in the WTG simulation of EC-Earthv1 with an SST of 301 K (see the light green curve in Figure 1k and and the value of P/P_{Ref} in Table 4). The WTG and DGW simulations of EC-Earthv1 with an SST of 301 K produces different signs of the circulation ($\Omega > 0$ and $P > P_{Ref}$ using the DGW method, compared to $\Omega < 0$ and $P < P_{Ref}$ using the WTG method; see Table 4).

At SSTs> 301 K, the mean precipitation rate is increased compared to the RCE in all the models using either the WTG or DGW method. These simulations produce uniform large-scale ascent in the simulated column, with the exceptions of the WTG simulations of ARPv6 and GISS-SCM, in which a thin layer of descent between 750 and 650 hPa does not prevent an increase in mean precipitation rate due to lower and upper tropospheric ascent (see the light green, orange, and red curves in Figures 1i and 1h).

For most models the circulation and precipitation increase monotonically with SST. For all CRMs using either the WTG or the DGW method the simulated column evolves toward a new quasi-equilibrium state with mean precipitation rate increasing non-linearly with SST, consistent with SCM results from *Sobel and Bretherton* [2000], and *Ramsay and Sobel* [2011]. In contrast, the SCMs show sensitivities of the mean precipitation rate to the SST which are not always monotonic (e.g. EC-Earthv1 using either the WTG or DGW method; solid red curves in Figures 3b and 3d).

Within an individual model, the sensitivity of precipitation rate to the SST depends on which large-scale parameterization method is used. An example is WRF which shows

a stronger sensitivity under the DGW method than under the WTG method (compared the dashed curves in Figures 3a and 3c). On the other hand, given one of the large-scale parameterization methods (either the WTG or DGW), the sensitivity of precipitation rate to the SST differs from model to model, and LMDzA using either the WTG or the DGW method is the model which produces the weakest sensitivity compared to all other models (solid blue curves in Figures 3b and 3d).

Despite the differences in the pressure velocity profiles, the mass-weighted vertically-integrated large-scale pressure velocity, Ω shows a fairly linear relationship with the mean precipitation rate (see Figure 4). However, a few SCMs show deviations from this linear relationship, particularly for simulations with warm SST (e.g., GISS-SCM using the WTG method; circles in Figure 4b).

4.2. Precipitation and Column relative humidity

In this section, we examine the relationship between precipitation and the column relative humidity (after here CRH) in our WTG and DGW simulations. CRH is calculated as the ratio of column-integrated water vapor to its saturation value. Figure 5 shows scatter plots of P versus CRH. To account for the variations in CRH of the RCE reference state, we consider Figure 6, which shows scatter plots of the ratios P/P_{Ref} versus CRH/CRH_{Ref}, where CRH_{Ref} is the column-integrated relative humidity of the RCE reference state. The values of P and CRH are those obtained at equilibrium in the WTG and DGW simulations of each of the models listed in Tables 1 and 2 with the values of SST ranging between 298 and 302 K.

Generally, the mean precipitation rate increases as CRH increases, except in the DGW simulations of LMDzA with SSTs $\leqslant$ 300.5 K in which CRH decreases while precipitation

rate increases (see left facing triangles in Figure 5d). The decrease of CRH with mean precipitation rate is unusual, but we do not investigate this further in this study.

In a large proportion of the models, there is a threshold value of CRH below which there is virtually no precipitation or strongly reduced precipitation rate (with respect to the value of the RCE reference state) and above which precipitation rate rapidly increases with CRH. Below this threshold, the WTG and DGW simulations show changes in mean precipitation rate that are relatively small for large changes in CRH. Above this threshold, a significant increase in precipitation rate is obtained, followed by a sharp pickup of mean precipitation rate as CRH increases further. The value of this threshold varies from one model to another and it also varies depending on the large-scale parameterization method used.

These relationships between CRH and mean precipitation rate are qualitatively similar to that seen in observations [e.g., *Bretherton et al.*, 2004; *Holloway and Neelin*, 2009] and in other idealized models [e.g., *Raymond and Zeng*, 2005; *Wang and Sobel*, 2011], but there are significant quantitative differences. For instance, the transition from near zero precipitation to rapid increase in precipitation with CRH is sharper in some models compared to others (e.g., compare P versus CRH in the WTG simulations of UMv7.8 and LMDzB; stars and right facing triangles in Figure 5b, respectively). Moreover, CRMs using either the WTG or DGW method produce very similar relationships between P and CRH, while SCMs show a much larger variety of relationships. When P and CRH are scaled by their reference values (see Figure 6), the CRMs produce a relatively tight relationship. The spread among SCMs is also clearly reduced, although considerable scatter remains. In general, P increases more rapidly with CRH in CRMs than in SCMs.

4.3. Budget analysis

We now analyze the budgets in order to clarify the differences among RCE, WTG, and DGW simulations. From the moisture budget equation, the changes in mean precipitation rate with respect to the value of the RCE reference state, ΔP, must be due to changes in surface evaporation with respect to the value of the RCE reference state, ΔE, and/or the moistening rate due to the large-scale circulation M_{LS}. Figures 7 and 8 show scatter plots of ΔP versus M_{LS} and scatter plots of ΔP versus ΔE, respectively.

Both CRMs and SCMs show fairly linear relationships between ΔP and M_{LS}. However, the slope is not one-to-one (dotted oblique line in Figure 7), which implies changes in surface evaporation as shown in Figure 8. ΔE increases with ΔP in a large proportion of the WTG and DGW simulations, and there are only a few simulations which show an enhancement of convective activity associated with a reduction in surface evaporation (e.g., WTG simulation of LaRC-CRM an SST of 300.5 K, dark green solid diamond in Figure 8a) or which show a suppression in convective activity associated with an increase in surface evaporation (e.g., the WTG simulation of EC-Earthv1 with SST of 300.5 K, dark green diamond in Figure 8b).

The sensitivity of surface fluxes (sum of sensible heat and latent heat fluxes) to changes in near-surface perturbation winds due to changes in convective activity has been somewhat constrained in this study by imposing a mean horizontal wind speed in the surface flux calculations. As a result, ΔE is generally much smaller than ΔP, such that changes in precipitation are largely balanced by the large-scale moistening rates. This is readily seen in Figures 7 and 8. For a large proportion of the simulations, the values of M_{LS} are about or more than two third the values of ΔP.

As in *Daleu et al.* [2015], we examine the relationship between ΔP and the normalized gross moist stability (NGMS), Γ. We followed *Raymond et al.* [2009] and defined Γ as the dimensionless number which relates the net lateral outflow of moist static energy from a convective region to a measure of the strength of convection in that region. That is

$$\Gamma = -\langle \overline{\omega} \partial \overline{h} / \partial p \rangle / L \langle \overline{\omega} \partial \overline{q} / \partial p \rangle, \tag{6}$$

with $\langle \cdot \rangle = \int_{p_s}^{p_{top}} \cdot dp/g$. h is the moist static energy, q is the specific humidity of water vapor, and L is the latent heat of vaporization. From the heat and moisture budget equations, a diagnostic equation for ΔP is

$$\Delta P = \frac{\Gamma + 1}{\Gamma} \Delta E + \frac{\Delta H + \Delta R}{\Gamma}, \tag{7}$$

with

$$\Gamma = -(M_{LS} + H_{LS})/M_{LS}, \tag{8}$$

and

$$H_{LS} = C_p \langle \partial \overline{T} / \partial t \rangle_{LS}, \quad and \quad M_{LS} = L_v \langle \partial \overline{q} / \partial t \rangle_{LS}. \tag{9}$$

ΔH and ΔR are respectively the changes in surface sensible heat flux and column-integrated radiative cooling rates with respect to the values of the RCE reference state, and H_{LS} and M_{LS} are the heating and moistening rates due to the diagnosed large-scale circulation respectively. The reader is referred to *Daleu et al.* [2015] for a derivation of equations 7 and 8.

As discussed above, ΔH is much smaller than ΔP. ΔR is also much smaller than ΔP as a result of imposing a fixed radiative cooling profile throughout most of the troposphere. Also, most of these simulations show that the sum of ΔH and ΔR is much smaller than

498 ΔE, such that $(\Gamma + 1)/\Gamma$ largely describes the strength of the relationship between ΔP
499 and ΔE (see equation 7).

500 For the WTG and DGW simulations which reproduce the RCE reference state to a
501 good approximation, Γ is a poor diagnostic since $M_{LS} + H_{LS}$ and M_{LS} are both close to
502 zero, consistent with a weak large-scale circulation. Figure 9 shows scatter plots of ΔP
503 versus Γ for the WTG and DGW simulations which result in significant large-scale ascent
504 at equilibrium. These are simulations which produce $P/P_{Ref} > 1.1$ with $\Omega > 0.4 \times 10^{-2}$
505 Pa s^{-1}. The values of Γ for the WTG and DGW simulations which result in significant
506 large-scale descent at equilibrium are not particularly relevant in this study.

507 Most CRM simulations which result in significant large-scale ascent have positive values
508 of Γ and the WTG and DGW simulations of LaRC-CRM with an SST of 300.5 K are
509 the only CRM simulations which have negative values of Γ (dark green solid diamond in
510 Figures 9a and 9c). In those simulations, M_{LS} is positive, so the negative value of Γ is a
511 result of a deficit of cooling over moistening rates (not shown). Among SCMs, simulations
512 with warm SSTs which produce significant large-scale ascent have positive values of Γ.
513 Negative values of Γ in some SCMs are the results of either large-scale ascent over a cold
514 SST (e.g., the WTG of GISS-SCM with an SST of 299.5 K; light blue circle in Figure 9b)
515 or large-scale ascent over a uniform SST (e.g., the DGW simulations of EC-Earthv1 over
516 a uniform SST of 300 K; black diamond in Figure 9d).

517 Most simulations which result in significant large-scale ascent have values of Γ ranging
518 between 0 and 1, with the exception of the few simulations with have negative values of
519 Γ (e.g., LaRC-CRM using the WTG method with an SST of 300.5 K; dark green solid

diamond in Figures 9a) and the few simulations which have $\Gamma > 1$ (e.g., LMDzA using the DGW with an SST of 300.5 K; dark green left facing triangle in Figure 9d).

Wang and Sobel [2011] and *Sessions et al.* [2015] found that Γ is a predictor of ΔP in the precipitating regime. In this study, only two models exhibit positive values of Γ which are a monotonically decreasing function of P or of the SST as in *Wang and Sobel* [2011]. These models are WRF and LEMv2.4 using either the WTG or the DGW method with SSTs$>$ 300 K; see dark green, light green, orange, and red solid circles and solid inverted triangles in Figures 9a and 9c. In contrast, all other models exhibit positive or negative values of Γ which are not directly related to P or SST.

5. Conclusions

In this international intercomparison project, we systematically compared the interactions between convection and large-scale circulations in various CRMs and SCMs using the WTG and DGW methods. The WTG method derives the large-scale circulation from buoyancy anomalies with a given relaxation time-scale [*Raymond and Zeng*, 2005; *Sobel et al.*, 2007; *Sessions et al.*, 2010; *Daleu et al.*, 2012] while the DGW method derives the large-scale circulation from the momentum equations [*Kuang*, 2008, 2011; *Romps*, 2012a, b]. The derived large-scale circulation couples a model to a reference state defined with profiles generated from previous RCE simulations of the same model. In *Daleu et al.* [2015], we analysed WTG and DGW simulations over a uniform SST. In this paper, we kept the reference state fixed and conducted WTG and DGW simulations with different values of SST in the simulated column. In both cases, we compared the results from various CRMs and SCMs using each large-scale parameterization method.

The WTG and DGW simulations with a cold (or a warm) SST result in lower (or higher) precipitation rates (compared to the value of the RCE reference state) in all CRMs and in a large proportion of the SCMs. In a few SCMs, a WTG simulation over a warm SST and a corresponding DGW simulation produce different signs of the circulation. In those SCMs, different signs of the circulation occur because the WTG simulation produces large-scale ascent over a cold SST or large-scale descent over a warm SST. The strength and the vertical structure of the large-scale pressure velocities that develop over non-uniform SSTs differs from model to model, with the largest inter-model variability obtained among SCMs. The large-scale pressure velocities also depend on which large-scale parameterization approach is used. In general, DGW simulations produce large-scale pressure velocity profiles which are smoother than those produced by WTG simulations, and consistent with the results of *Wang et al.* [2013], DGW simulations generally produce large-scale pressure velocity profiles which are less top-heavy compared to those produced by WTG simulations.

In comparing model behavior for a given method of the large-scale parameterization (either WTG or DGW), we found that the sensitivity of precipitation rate to the SST differs from model to model. Within an individual model, the sensitivity also differs depending on which large-scale parameterization method is used. All CRMs and five out of the seven SCMs show a monotonic increase of mean precipitation rate with SST using either the WTG or DGW method. A similar relationship between precipitation rate and SST was produced in *Sobel and Bretherton* [2000] and *Ramsay and Sobel* [2011]. The other two SCMs show sensitivity of the mean precipitation rate with SST which is not always monotonic. CRMs show a fairly linear relationship between mean precipitation

564 rate and the amplitude of the diagnosed vertically-integrated large-scale circulation, while
565 a few SCMs show deviations from this linear relationship, particularly for simulations with
566 warm SST.

567 Precipitation is an increasing function of the column relative humidity, with the former
568 increasing rapidly as the latter passes a threshold. A similar relationship is found in other
569 numerical modeling studies [*Wang and Sobel*, 2011; *Raymond and Zeng*, 2005], and is
570 consistent with observations [*Bretherton et al.*, 2004; *Holloway and Neelin*, 2009]. All
571 CRMs using either the WTG or DGW method show very similar relationships between
572 mean precipitation rate and column-relative humidity. SCMs show a much wider range
573 of relationships between precipitation rate and column-relative humidity, although this
574 spread is reduced when values are normalized by their RCE values.

575 In our WTG and DGW simulations, the change in precipitation with respect to the
576 value of the RCE reference column is largely balanced by the moistening rate due to the
577 large-scale circulation. We estimated the NGMS for simulations with significant large-
578 scale ascent. A large proportion of the simulations exhibited positive values of NGMS,
579 ranging between 0 and 1, and only few simulations exhibit negative values of NGMS or
580 values of NGMS that approach 1.5. Although two of the CRMs exhibited positive values
581 of NGMS which are decreasing functions of the mean precipitation rate (or decreasing
582 function of the SST), consistent with the results of *Wang and Sobel* [2011], the other
583 CRMs and all of the SCMs exhibited negative or positive values of NGMS, with no direct
584 relation to the mean precipitation rate or the SST.

585 The results from this intercomparison project are important for understanding the two-
586 way interaction between convection and large-scale tropical dynamics and also for inter-

preting discrepancies between the results reported in the literature. Our results suggested that the discrepancies between the published results can be related to the choice of the large-scale parameterization method and the details of its implementation. For instance, we found that an individual model can produce different equilibrium states depending on the large-scale parameterization method used, and we also showed that the results using the WTG method are very sensitive to the details of the implementation of the WTG method. Moreover, our results also suggested that the discrepancies between the published results can be related to the differences in the physics of the convection models, since the exact implementation of either the WTG or DGW method in different CRMs and SCMs has resulted in different model behaviors at equilibrium. However, noting that different CRMs under parameterized large-scale circulation behave broadly in the similar way while SCMs produce a much larger variation of behaviors, comparison between CRMs and SCMs behavior under parameterized large-scale circulation may be a useful tool for trying to reduce biases or improve the SCMs or a useful tool when developing and testing parameterization schemes. Further study may compare models and large-scale parameterization methods with interactive radiation and/or interactive surface.

Acknowledgments. C.L.D., R.S.P., and S.J.W. thank the UK Met Office for the availability of the LEM at version 2.4 and SCM version 7.8 of the UK Met Office Unified Model. C.L.D. was supported by NERC, grant NE/K004034/1. S.J.W. was supported by the NCAS, a NERC collaborative center. The New Mexico Tech group thanks Carlos Lopez Carrillo, Ana Juračić, and Stipo Sentić for model output analysis and for continual discussions on the tropical atmosphere. We also thank Raúl Morales-Juberías for use of the Pelican beowulf cluster. S.L.S. acknowledges support from U.S. National Sci-

ence Foundation Grants AGS-1056254 and AGS-1342001, and NM EPSCoR. M.J.H. was supported by U. S. National Science Foundation Grant 1342001. A.H.S .and S.W. were partially supported by NSF grant AGS-1062206. The WRF simulations were carried out on the Yeti Shared HPC Cluster at Columbia University. G.B. thanks Isabelle Beau, Antoinette Alias, David Saint-Martin, Jean-Yves Grandpeix, Marie-Pierre Lefebvre and the CNRS/INSU-LEFE project DEPHY and the European Union FP7 project EMBRACE. D.K. appreciates the NASA/GISS modeling group, especially Maxwell Kelley, Mao-Sung Yao, and Anthony Del Genio, for their invaluable and unlimited supports. D.K. and A.H.S. were supported by the NASA grant NNX13AM18G and the Korea Meteorological Administration Research and Development Program under Grant CATER 2013-3142. LaRC CRM-IPHOC was partially supported by DOE Atmospheric System Research Program under Interagency agreements DE-SC0005450 and DE-SC0008779. The computation resources were provided by SSAI Icluster and LaRC Kcluster. P.P., A.P.S. and L.U. were supported by the European Commissions Seventh Framework Programme, under Grant Agreement number 282672, EMBRACE project. Data used for this research are available upon request from the corresponding author; please send requests via email to c.daleu@reading.ac.uk.

References

Bretherton, C., and P. Smolarkiewcz (1989), Gravity waves, compensating subsidence and detrainment around cumulus clouds, *J. Atmos. Sci.*, *46*, 740–759.

Bretherton, C., P. Blossey, and M. Khairoutdinov (2005), An energy-balance analysis of deep convective self-aggregation above uniform SST, *J. Atmos. Sci.*, *62*, 4273–4292.

631 Bretherton, C. S., M. E. Peters, and L. E. Back (2004), Relationships between water
632 vapor path and precipitation over the tropical oceans, *J. Clim.*, *17*, 1517–1528.
633 Cheng, A., and K.-M. Xu (2006), Simulation of shallow cumuli and their transition to
634 deep convective clouds by cloud-resolving models with different third-order turbulence
635 closures, *Q. J. R. Meteorol. Soc.*, *132*, 359–382.
636 Daleu, C., S. Woolnough, and R. Plant (2012), Cloud-resolving model simulations with
637 one and two-way couplings via the weak-temperature gradient approximation, *J. Atmos.*
638 *Sci.*, *69*, 3683–3699.
639 Daleu, C., S. Woolnough, and R. Plant (2014), Transition from suppressed to active
640 convection modulated by a weak-temperature gradient derived large-scale circulation,
641 *J. Atmos. Sci.*, *72*, 834–853.
642 Daleu, C., et al. (2015), Intercomparison of methods of coupling between convection and
643 large-scale circulation: I. comparison over uniform surface conditions, *J. Adv. Model.*
644 *Earth. Syst.*
645 Davies, T., M. Cullen, A. Malcolm, M. Mawson, A. Staniforth, A. White, and N. Wood
646 (2005), A new dynamical core for the Met Office's global and regional modelling of the
647 atmosphere, *Q. J. R. Meteorol. Soc.*, *131*, 1759–1782.
648 Dufresne, J.-L., et al. (2013), Climate change projections using the IPSL-CM5 earth
649 system model: From CMIP3 to CMIP5, *Clim. Dyn.*, *40*, 2123–2165.
650 Edman, J. P., and D. M. Romps (2015), Self-consistency tests of large-scale dynamics
651 parameterizations for single-column modeling, *J. Adv. Model. Earth. Syst.*, *7*, 320–334.
652 Hazeleger, W., et al. (2010), EC-Earth: A seamless earth-system prediction approach in
653 action, *Bull. Am. Meteorol. Soc.*, *91*, 1357–1363.

654 Herman, M. J., and D. J. Raymond (2014), WTG cloud modeling with spectral decom-
655 position of heating, *J. Adv. Model. Earth. Syst.*, *6*, 1121–1140.

656 Holloway, C., S. Woolnough, and G. Lister (2012), Precipitation distributions for explicit
657 versus parametrized convection in a large-domain high-resolution tropical case study,
658 *Q. J. R. Meteorol. Soc.*, *138*, 1692–1708.

659 Holloway, C. E., and J. D. Neelin (2009), Moisture vertical structure, column water vapor,
660 and tropical deep convection, *J. Atmos. Sci.*, *66*, 1665–1683.

661 Kuang, Z. (2008), Modeling the interaction between cumulus convection and linear grav-
662 ity waves using a limited-domain cloud system-resolving model, *J. Atmos. Sci.*, *65*,
663 576–591.

664 Kuang, Z. (2011), The wavelength dependence of the gross moist stability and the scale
665 selection in the instability of column-integrated moist static energy, *J. Atmos. Sci.*, *68*,
666 61–74.

667 Lafore, J. P., et al. (1997), The Meso-NH atmospheric simulation system. Part I: Adi-
668 abatic formulation and control simulations, in *Ann. Geophys*, vol. 16, pp. 90–109,
669 Springer.

670 Mapes, B., and X. Wu (2001), Notes and correspondence. Convective eddy momentum
671 tendencies in long cloud-resolving model simulations, *J. Atmos. Sci.*, *58*, 517–526.

672 Mapes, B. E., and R. A. Houze (1995), Diabatic divergence profiles in western Pacific
673 mesoscale convective systems, *J. Atmos. Sci.*, *52*, 1807–1828.

674 Pauluis, O., and S. Garner (2006), Sensitivity of radiative-convective equilibrium simu-
675 lations to horizontal resolution, *J. Atmos. Sci.*, *63*, 1910–1923.

Petch, J., and M. Gray (2001), Sensitivity studies using a cloud-resolving model simulation of the tropical west Pacific, *Q. J. R. Meteorol. Soc.*, *127*, 2287–2306.

Ramsay, H., and A. Sobel (2011), Effects of relative and absolute sea surface temperature on tropical cyclone potential intensity using a single-column model, *J. Clim.*, *24*, 183–193.

Raymond, D., and X. Zeng (2005), Modelling tropical atmospheric convection in the context of the weak temperature gradient approximation, *Q. J. R. Meteorol. Soc.*, *131*, 1301–1320.

Raymond, D. J., S. L. Sessions, A. H. Sobel, and Ž. Fuchs (2009), The mechanics of gross moist stability, *J. Adv. Model. Earth. Syst.*, *1*.

Robe, F., and K. Emanuel (2001), The effect of vertical wind shear on radiative-convective equilibrium states, *J. Atmos. Sci.*, *58*, 1427–1445.

Romps, D. (2012a), Weak pressure gradient approximation and its analytical solutions, *J. Atmos. Sci.*, *69*, 2835–2845.

Romps, D. M. (2012b), Numerical tests of the weak pressure gradient approximation, *J. Atmos. Sci.*, *69*, 2846–2856.

Schmidt, G. A., et al. (2014), Configuration and assessment of the GISS modele2 contributions to the CMIP5 archive, *J. Adv. Model. Earth. Syst.*, *6*, 141–184.

Sessions, S., S. Sugaya, D. Raymond, and A. Sobel (2010), Multiple equilibria in a cloud-resolving model using the weak temperature gradient approximation, *J. Geophys. Res.*, *115*, D12,110.

Sessions, S. L., M. J. Herman, and S. Sentić (2015), Convective response to changes in the thermodynamic environment in idealized weak temperature gradient simulations, *J.*

699 *Adv. Model. Earth. Syst.*

700 Shutts, G., and M. Gray (1994), A numerical modelling study of the geostrophic adjust-
701 ment process following deep convection, *Q. J. R. Meteorol. Soc.*, *120*, 1145–1178.

702 Skamarock, W. C., J. B. Klemp, J. Dudhia, D. O. Gill, D. M. Barker, W. Wang, and
703 J. G. Powers (2008), A description of the advanced research WRF version 3, *Tech. rep.*,
704 DTIC Document.

705 Sobel, A., and C. Bretherton (2000), Modeling tropical precipitation in a single column,
706 *J. Clim.*, *13*, 4378–4392.

707 Sobel, A., G. Bellon, and J. Bacmeister (2007), Multiple equilibria in a single-column
708 model of the tropical atmosphere, *Geophys. Res. Lett.*, *34*, L22,804.

709 Tao, W., J. Simpson, C. Sui, C. Shie, B. Zhou, K. Lau, and M. Moncrieff (1999), Equi-
710 librium states simulated by cloud-resolving models, *J. Atmos. Sci.*, *56*, 3128–3139.

711 Tompkins, A. (2000), The impact of dimensionality on long-term cloud-resolving model
712 simulations, *Mon. Weather Rev.*, *128*, 1521–1535.

713 Voldoire, A., et al. (2013), The CNRM-CM5. 1 global climate model: description and
714 basic evaluation, *Clim. Dyn.*, *40*, 2091–2121.

715 Wang, S., and A. Sobel (2011), Response of convection to relative sea-surface tempera-
716 ture: Cloud-resolving simulations in two and three dimensions, *J. Geophys. Res.*, *116*,
717 D11,119.

718 Wang, S., and A. Sobel (2012), Impact of imposed drying on deep convection in a cloud-
719 resolving model, *J. Geophys. Res.*, *117*.

720 Wang, S., A. H. Sobel, and Z. Kuang (2013), Cloud-resolving simulation of TOGA-
721 COARE using parameterized large-scale dynamics, *J. Geophys. Res.*, *118*, 6290–6301.

722 Yano, J.-I., and M. Bonazzola (2009), Scale analysis for the large-scale tropical atmo-
723 spheric dynamics, *J. Atmos. Sci.*, *66*, 159–172.

Model type	Cloud-Resolving Models (CRMs)				
Modelling group	Columbia University	CNRM-GAME	NASA	New Mexico Tech	UK Met Office
Model ID	WRF	MesoNH	LaRC-CRM	NMTCMv3	LEMv2.4
Symbol	●	▲	♦	■	▼
Contributor	S. Wang	P. Peyrille	A. Cheng	M. J. Herman	C. Daleu
Country	U.S.	France	U.S.	U.S.	UK
Dimension	3D	3D	2D	2D	2D
Hor. size (km)	190×190	150×150	256	200	128
Hor. res (km)	2×2	3×3	4	1	0.5
N° of levels in the vertical	49	46	30	81	59
P_{Ref} (mm d^{-1})	4.71	4.63	4.60	4.35	4.82

Table 1. *List of cloud-resolving models (CRMs) that participated in this study. The symbols serve as a legend for results presented in Section 4. P_{Ref} is the mean precipitation rate obtained in the radiative-convective equilibrium simulation of each CRM with an SST of* 300 *K.*

Model type	Single-Column Models (SCMs)						
Modelling group	LMD/IPSL		NASA	CNRM-GAME	UK Met Office	Koninklikj Nederlands Meteorologisch Insituut	
Model ID	LMDzA	LMDzB	GISS-SCM	ARPEGEv6 (ARPv6)	UMv7.8	EC-Earthv1	EC-Earthv3
Symbol	$\triangleleft$	$\triangleright$	$\circ$	$\triangledown$	$\star$	$\diamond$	$\square$
Contributor	G. Bellon	G. Bellon	D. Kim	G. Bellon	C. Daleu	P. Siebesma	P. Siebesma
Country	France	France	U.S.	France	UK	NL	NL
N° of levels in the vertical	39	39	40	91	63	62	62
P_{Ref} (mm d^{-1})	4.38	4.39	4.58	3.71	4.76	4.53	4.15

Table 2. *List of single-column models (SCMs) that participated in this study. The symbols serve as a legend for results presented in Section 4. P_{Ref} is the mean precipitation rate obtained in the radiative-convective equilibrium simulation of each SCM with an SST of* 300 *K.*

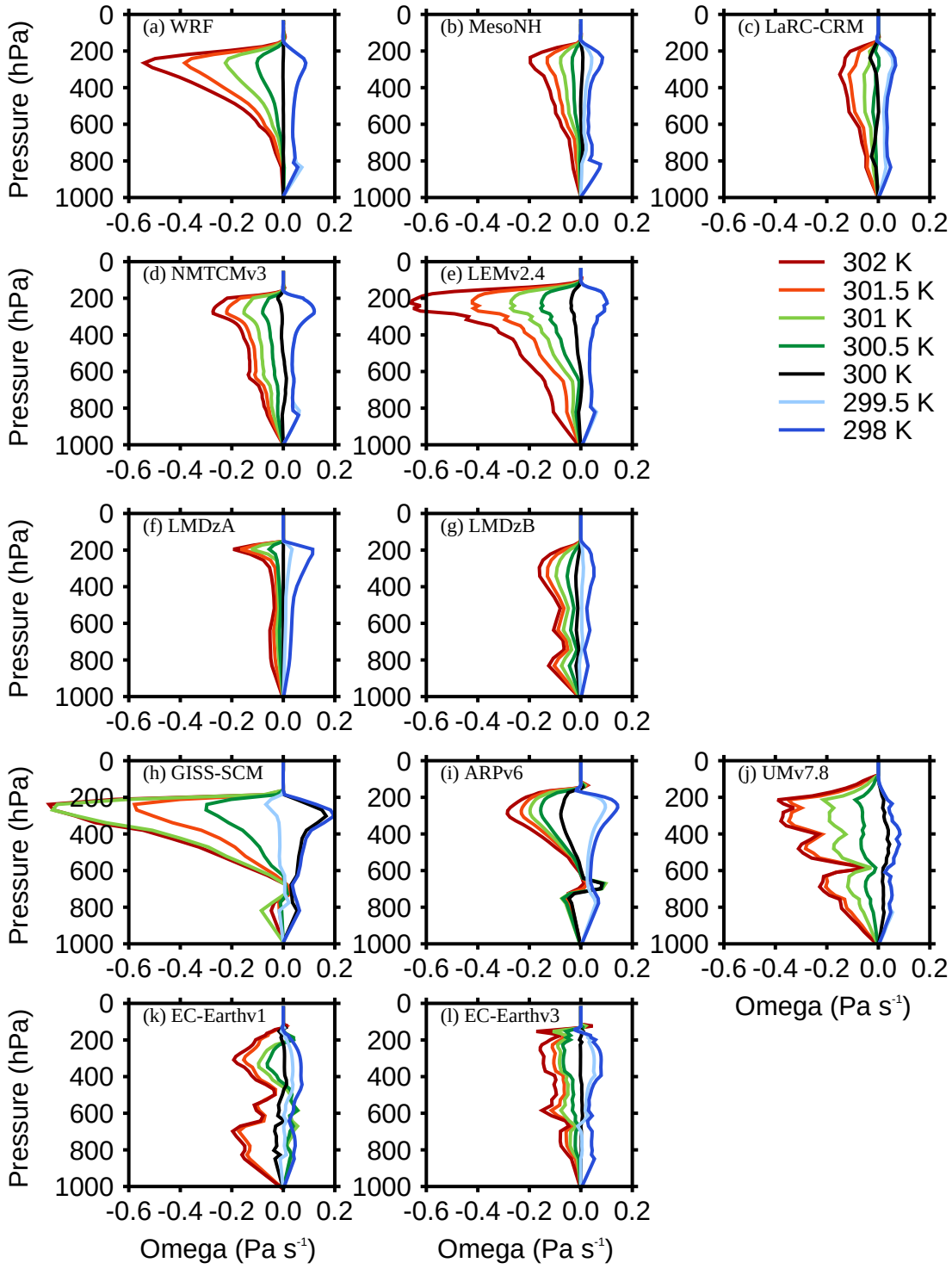

Figure 1. *Large-scale pressure velocities obtained at equilibrium in the WTG simulations with an SST of* 298 *K (dark blue),* 299.5 *K (light blue),* 300 *K (black),* 300.5 *K (dark green),* 301 *K (light green),* 301.5 *K (orange),* 302 *K (red). Results are shown for the (a, b, c, d and e) CRMs and (f, g, h, i, j, k and l) SCMs. For each model, the reference profiles are their own RCE profiles at* 300 *K.*

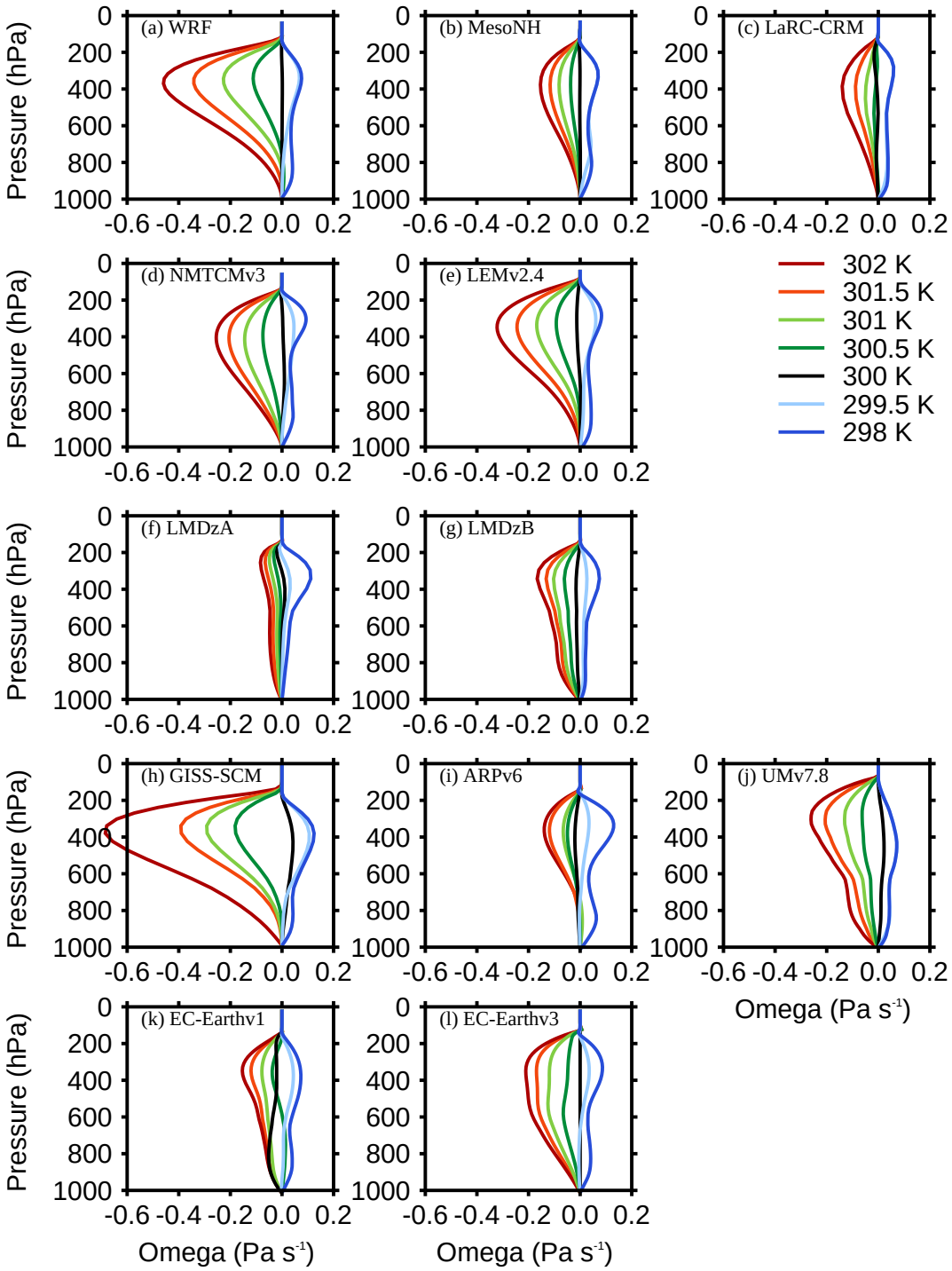

Figure 2. *As in Figure 1, but for the equilibrium in the DGW simulations.*

Model-CRMs	WTG or DGW	P/P_{Ref} or Ω	SST= 298 K	SST= 299.5 K	SST= 300 K	SST= 300.5 K	SST= 301 K	SST= 301.5 K	SST= 302 K
WRF	WTG	P/P_{Ref}	0.000	0.000	**1.020**	1.610	2.370	3.330	4.240
		Ω	-4.210	-4.420	**0.180**	2.990	6.670	11.230	15.520
	DGW	P/P_{Ref}	0.000	0.420	**1.008**	1.950	3.350	5.100	6.970
		Ω	-4.089	-2.575	**0.110**	4.180	9.485	15.547	22.235
MesoNH	WTG	P/P_{Ref}	0.002	0.529	0.896	1.303	1.714	2.220	2.857
		Ω	-4.079	-1.577	**-0.290**	1.391	3.176	5.221	7.839
	DGW	P/P_{Ref}	0.009	0.015	**0.970**	1.425	2.073	2.594	3.190
		Ω	-3.739	-3.461	**0.060**	1.803	4.145	6.0356	8.113
LaRC-CRM	WTG	P/P_{Ref}	0.006	0.276	1.200	1.233	1.908	2.824	3.322
		Ω	-3.549	-2.621	0.970	0.887	2.994	6.111	7.856
	DGW	P/P_{Ref}	0.000	0.084	1.102	1.233	1.757	2.394	3.282
		Ω	-3.563	-3.293	0.610	0.794	2.555	4.671	7.558
NMTCMv3	WTG	P/P_{Ref}	0.000	0.001	**1.028**	1.830	2.679	3.352	3.912
		Ω	-4.517	-4.621	**0.100**	3.303	6.570	9.221	11.317
	DGW	P/P_{Ref}	0.000	0.445	0.896	1.954	3.090	4.044	4.887
		Ω	-4.291	-2.266	**-0.388**	3.696	7.665	11.073	13.917
LEMv2.4	WTG	P/P_{Ref}	0.000	0.000	1.240	1.886	2.997	4.159	6.124
		Ω	-4.588	-4.668	1.110	5.471	9.745	15.162	24.048
	DGW	P/P_{Ref}	0.000	0.413	1.117	1.923	2.888	3.953	5.111
		Ω	-4.460	-2.658	0.464	4.129	8.103	12.436	17.031

Table 3. *Table showing the numerical values of* Ω *(*$\times 10^{-2}$ *Pa* s^{-1}*) and* P/P_{Ref} *for WTG and DGW simulations with different values of SST in the simulated column. Results in bold correspond to* $|\Omega| < 0.4 \times 10^{-2}$ *Pa* s^{-1} *(or* $\overline{\omega} \approx 0$*) or* $0.9 < P/P_{Ref} < 1.1$*. If both* Ω *and* P/P_{Ref} *are bold, the simulation with large-scale parameterization reproduces the RCE state to a good approximation.*

Model-SCMs	WTG or DGW	P/P_{Ref} or Ω	SST= 298 K	SST= 299.5 K	SST= 300 K	SST= 300.5 K	SST= 301 K	SST= 301.5 K	SST= 302 K
LMDzA	WTG	P/P_{Ref}	0.176	0.790	**0.997**	1.313	1.520	1.829	2.192
		Ω	-4.071	-1.037	**-0.015**	1.385	2.240	3.387	4.806
	DGW	P/P_{Ref}	0.15	0.804	**0.982**	1.187	1.530	1.874	2.201
		Ω	-4.145	-0.972	**-0.065**	0.931	2.169	3.437	4.652
LMDzB	WTG	P/P_{Ref}	0.362	0.929	1.290	1.694	2.273	2.729	3.127
		Ω	-2.670	-0.30	1.180	2.992	5.475	7.470	9.193
	DGW	P/P_{Ref}	0.248	0.638	1.269	1.922	2.537	2.940	3.437
		Ω	-3.325	-1.462	1.030	3.676	6.153	7.726	9.689
GISS-SCM	WTG	P/P_{Ref}	0.044	1.200	0.180	3.325	4.161	2.833	5.605
		Ω	-6.888	1.100	-5.700	7.371	24.25	14.760	25.022
	DGW	P/P_{Ref}	0.021	0.330	0.820	2.201	3.498	4.319	8.296
		Ω	-6.095	-4.395	-2.180	7.566	12.837	17.475	34.335
ARPv6	WTG	P/P_{Ref}	0.003	0.000	1.530	1.920	2.067	2.132	2.368
		Ω	-5.486	-3.852	2.230	5.055	6.132	7.210	8.658
	DGW	P/P_{Ref}	0.000	0.832	1.260	1.442	1.464	2.098	2.223
		Ω	-5.853	-1.122	0.972	2.046	2.340	5.0256	5.673
UMv7.8	WTG	P/P_{Ref}	0.022	0.036	0.470	2.228	4.002	6.129	6.743
		Ω	-4.528	-4.600	-2.130	4.053	10.751	18.537	20.610
	DGW	P/P_{Ref}	0.003	0.0343	0.700	2.257	3.350	4.534	5.623
		Ω	-4.465	-4.437	-1.240	3.875	7.734	12.104	15.878
EC-Earthv1	WTG	P/P_{Ref}	0.011	0.792	1.420	0.529	0.558	3.682	4.101
		Ω	-4.060	-1.262	0.990	-0741	-0.192	9.275	10.855
	DGW	P/P_{Ref}	0.002	0.662	1.920	1.024	2.271	2.807	3.170
		Ω	-4.117	-1.737	2.990	0.583	4.713	6.736	8.187
EC-Earthv3	WTG	P/P_{Ref}	0.003	0.577	**0.940**	1.720	2.202	2.648	3.430
		Ω	-4.209	-1.860	**-0.135**	2.927	4.611	6.008	8.523
	DGW	P/P_{Ref}	0.0122	0.813	**1.014**	2.191	3.448	4.344	5.087
		Ω	-4.280	-0.986	**0.146**	3.873	8.138	11.061	13.460

Table 4. *Same as Table 3, but lists SCM results.*

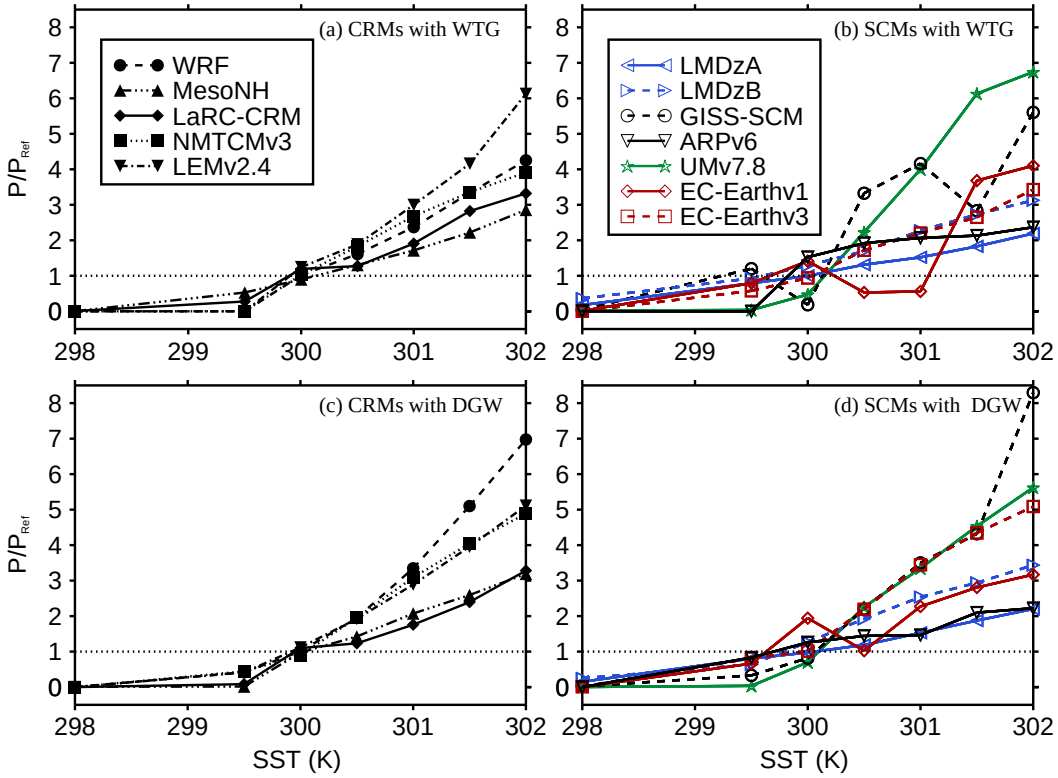

Figure 3. *P/P_{Ref} versus SST. The values of P are those obtained at equilibrium in the (top) WTG and (bottom) DGW simulations. Results are shown for (left) CRMs and (right) SCMs. Symbol definitions are as in Tables 1 and 2.*

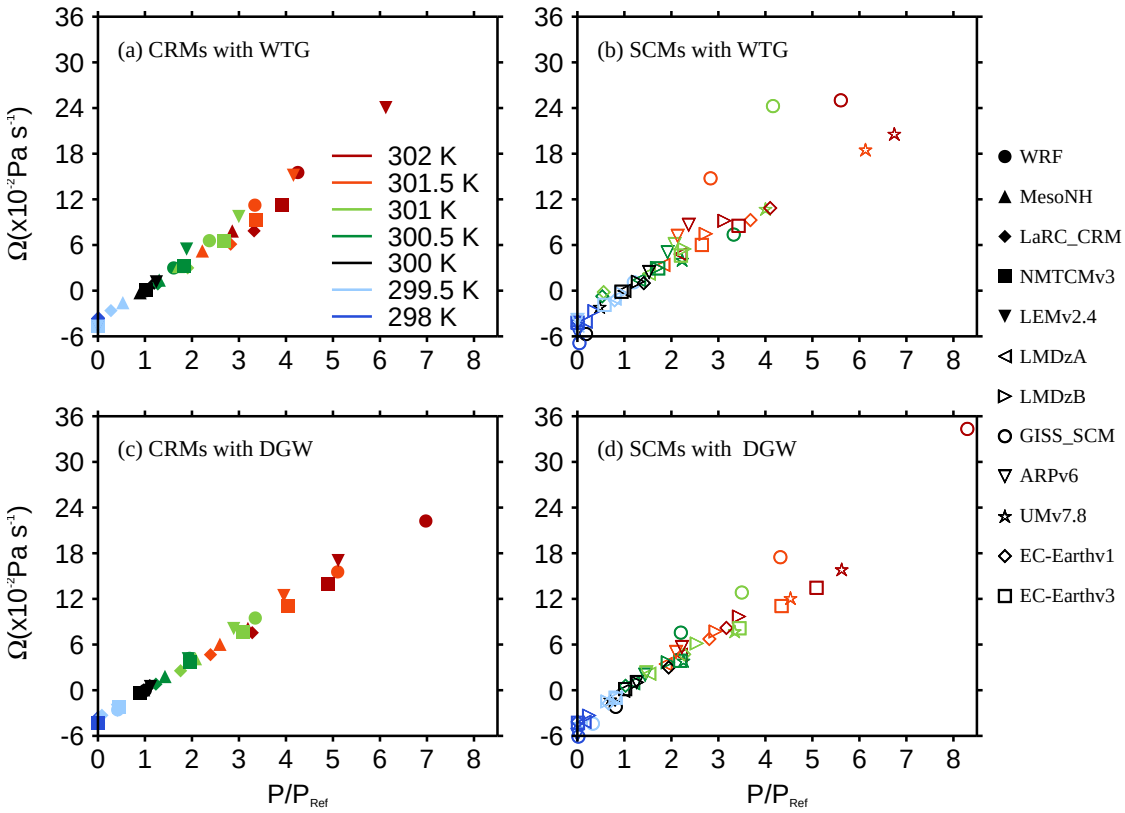

Figure 4. *Scatter plots of* Ω *versus* P/P_{Ref}. *Results are those obtained at equilibrium in the (top) WTG and (bottom) DGW simulations with an SST of* 298 *K (dark blue),* 299.5 *K (light blue),* 300 *K (black),* 300.5 *K (dark green),* 301 *K (light green),* 301.5 *K (orange), and* 302 *K (red). Results are shown for (left) CRMs and (right) SCMs. Symbol definitions are as in Tables 1 and 2.*

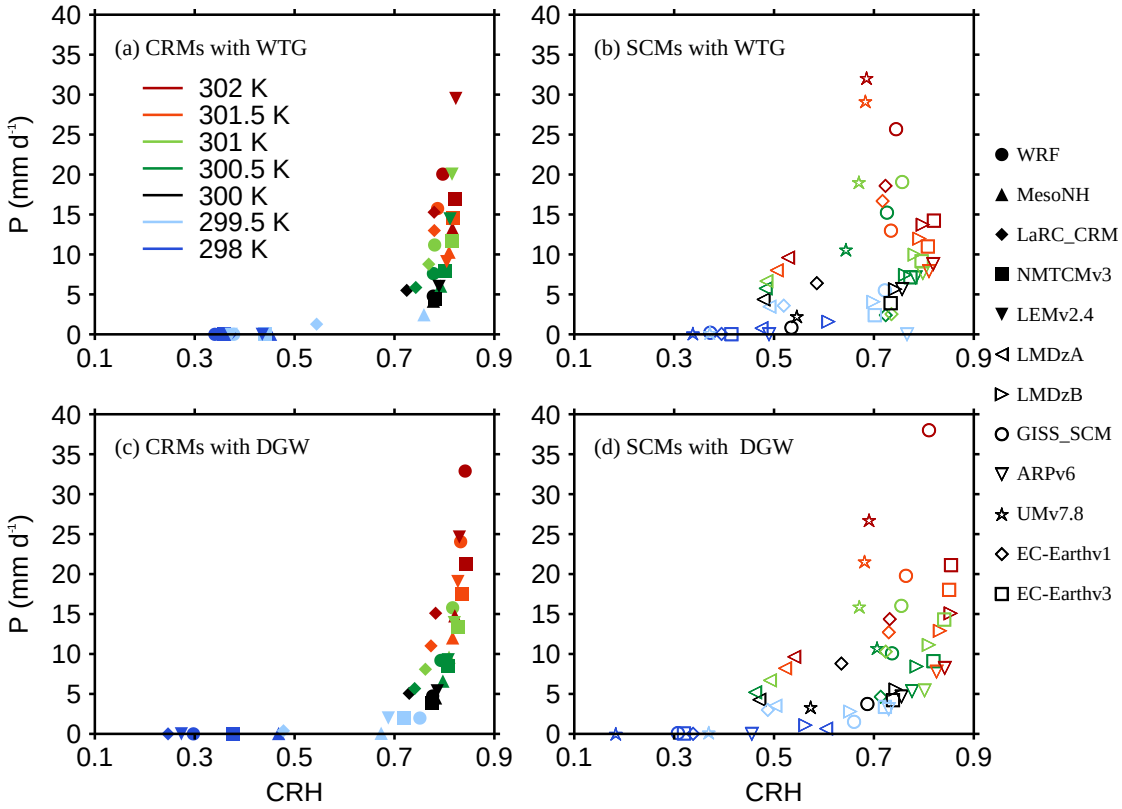

Figure 5. *Scatter plots of P versus CRH (column relative humidity; the column-integrated water vapor divided by its saturation value). The results are those obtained at equilibrium in the (top) WTG and (bottom) DGW simulations with an SST of* 298 *K (dark blue),* 299.5 *K (light blue),* 300 *K (black),* 300.5 *K (dark green),* 301 *K (light green),* 301.5 *K (orange), and* 302 *K (red). Results are shown for (left) CRMs and (right) SCMs. Symbol definitions are as in Tables 1 and 2.*

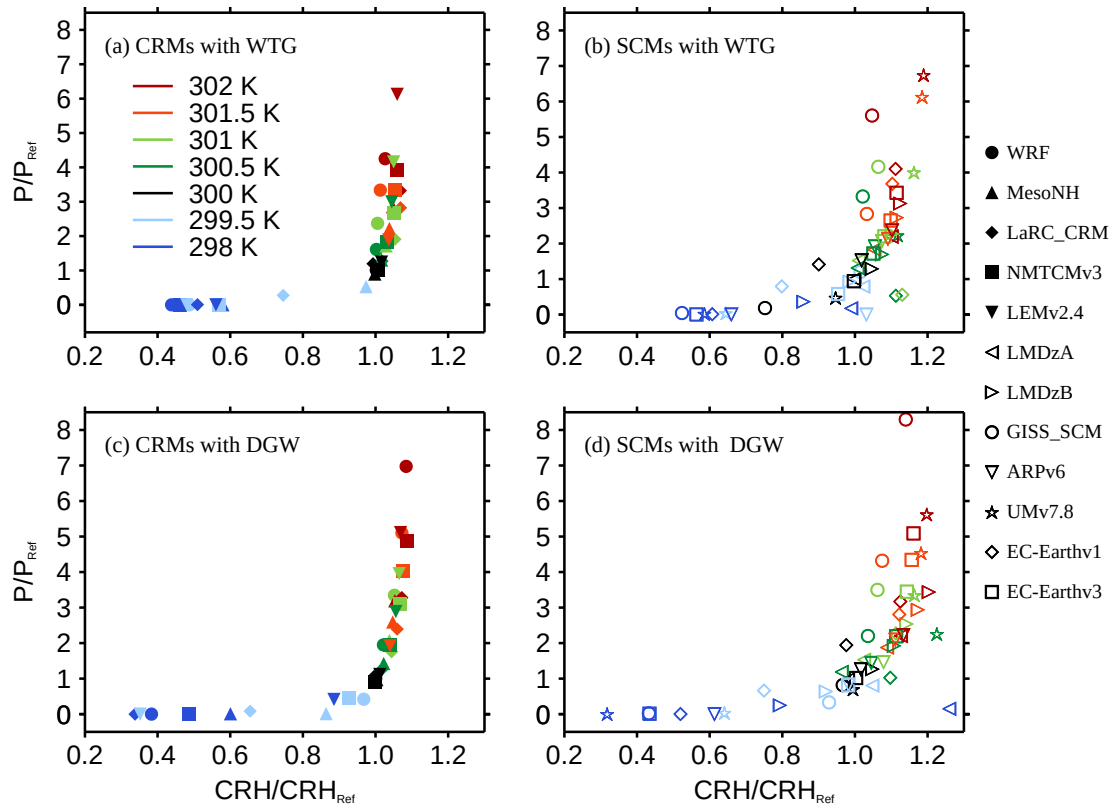

Figure 6. *Scatter plots of P/P_{Ref} versus CRH/CRH_{Ref}, where CRH_{Ref} is the column relative humidity of the corresponding RCE reference state. The results are those obtained at equilibrium in the (top) WTG and (bottom) DGW simulations with an SST of* 298 *K (dark blue),* 299.5 *K (light blue),* 300 *K (black),* 300.5 *K (dark green),* 301 *K (light green),* 301.5 *K (orange), and* 302 *K (red). Results are shown for (left) CRMs and (right) SCMs. Symbol definitions are as in Tables 1 and 2.*

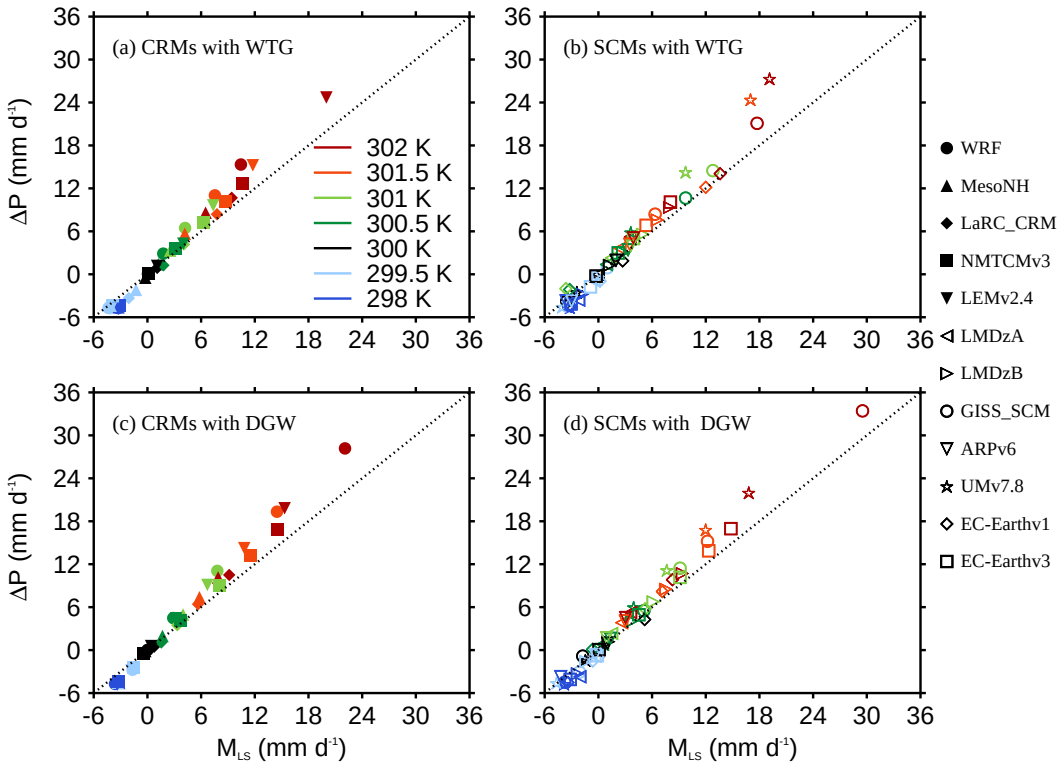

Figure 7. *Scatter plots of ΔP versus M_{LS}. The results are those obtained at equilibrium in the (top) WTG and (bottom) DGW simulations with an SST of* 298 *K (dark blue),* 299.5 *K (light blue),* 300 *K (black),* 300.5 *K (dark green),* 301 *K (light green),* 301.5 *K (orange), and* 302 *K (red). Results are shown for (left) CRMs and (right) SCMs. The dotted oblique line corresponds to $\Delta P = M_{LS}$. Symbol definitions are as in Tables 1 and 2.*

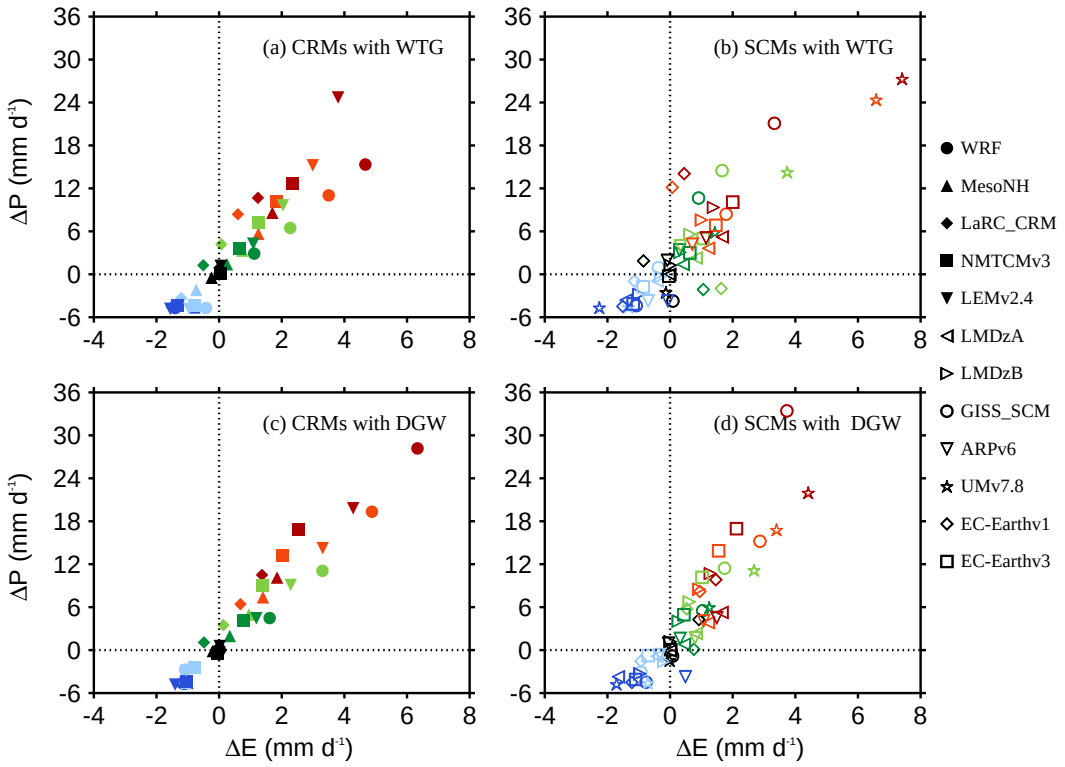

Figure 8. *Scatter plots of ΔP versus ΔE. Results are those obtained at equilibrium in the (top) WTG and (bottom) DGW simulations over an SST of* 298 *K (dark blue),* 299.5 *K (light blue),* 300 *K (black),* 300.5 *K (dark green),* 301 *K (light green),* 301.5 *K (orange), and* 302 *K (red). Results are shown for (left) CRMs and (right) SCMs. Symbol definitions are as in Tables 1 and 2.*

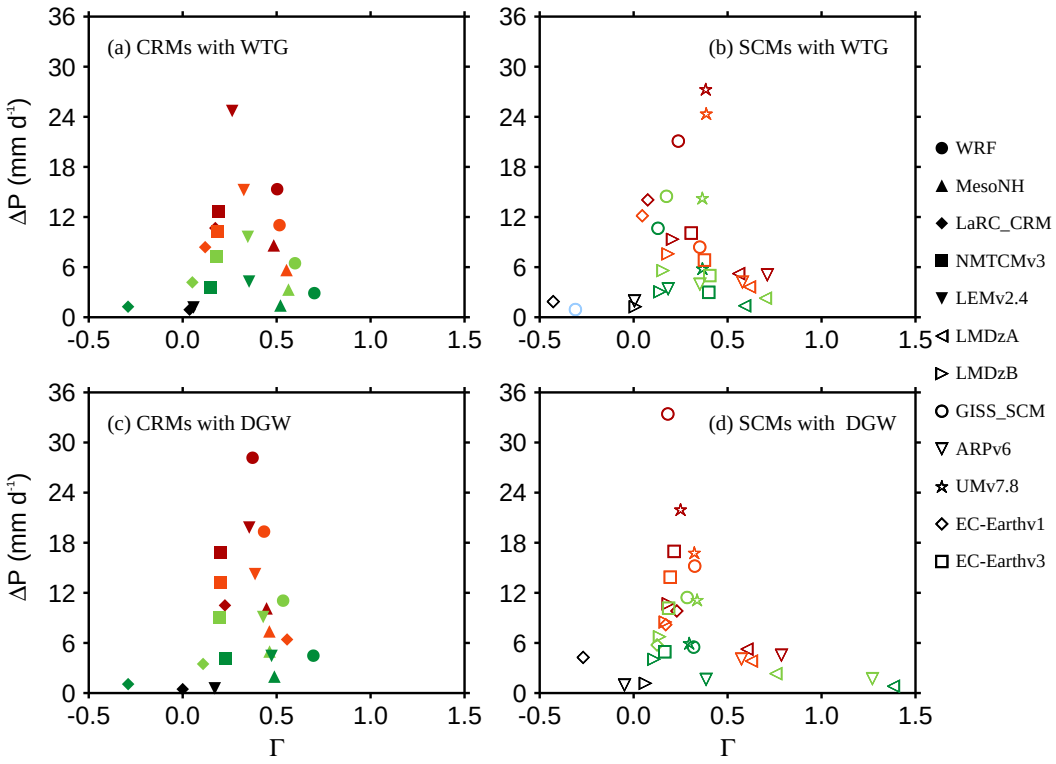

Figure 9. *Scatter plots of ΔP versus Γ. Results are those obtained at equilibrium in the (top) WTG and (bottom) DGW simulations over an SST of 298 K (dark blue), 299.5 K (light blue), 300 K (black), 300.5 K (dark green), 301 K (light green), 301.5 K (orange), and 302 K (red). Results are shown for (left) CRMs and (right) SCMs, and for WTG and DGW simulations which produce significant large-scale ascent only ($P/P_{Ref} > 1.1$ and $\Omega > 0.4 \times 10^{-2}$ Pa s^{-1}). Symbol definitions are as in Tables 1 and 2.*